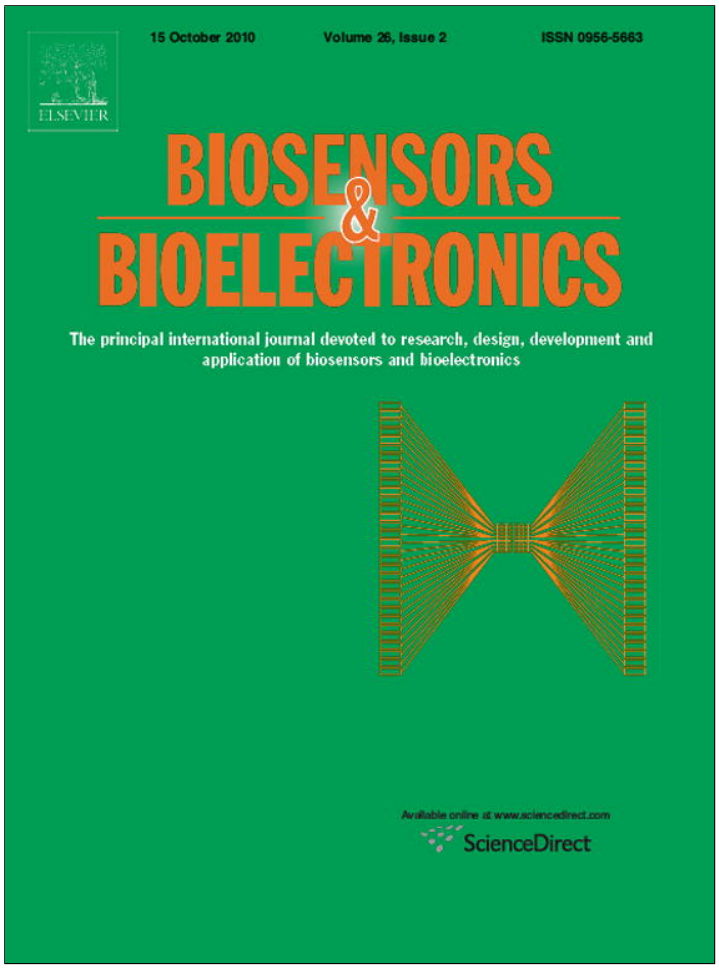

Biosensors and Bioelectronics 26 (2010) 809–814

Contents lists available at ScienceDirect

Biosensors and Bioelectronics

journal homepage: www.elsevier.com/locate/bios

# Reading microdots of a molecularly imprinted polymer by surface-enhanced Raman spectroscopy

Keren Kantarovich[a], Inbal Tsarfati[b], Levi A. Gheber[b], Karsten Haupt[c], Ilana Bar[a,*]

[a] Department of Physics, Ben-Gurion University of the Negev, Beer-Sheva 84105, Israel
[b] Department of Biotechnology Engineering, Ben-Gurion University of the Negev, Beer-Sheva 84105, Israel
[c] Compiègne University of Technology, UMR CNRS 6022, France

ARTICLE INFO

*Article history:*
Received 23 November 2009
Received in revised form 13 May 2010
Accepted 16 June 2010
Available online 23 June 2010

*Keywords:*
Molecularly imprinted polymer
Surface-enhanced Raman scattering
Nano-fountain pen

ABSTRACT

Writing a molecularly imprinted polymer (MIP) by nano-fountain pen on surface-enhanced Raman scattering (SERS)-active surfaces resulted in site-controlled arrays of microdots of approximately 6–12 μm in diameter. The monitoring of SERS spectra with a micro-Raman system enabled examining the uptake and release of the *S*-propranolol imprinting template and allowed imaging individual dots as well as multiple dots in an array, revealing the distribution of the imprinted polymer. This distribution was confirmed by atomic force microscopy, showing that even in dots of <300 nm thickness, corresponding to MIP volumes of 0.5 fl, significantly less than previously reported, the target analyte could be detected and identified. This study shows that nanolithography techniques combined with SERS might open the possibility of miniaturized arrayed MIP sensors with label-free, specific and quantitative detection.



## 1. Introduction

Endpoint determination of analytes in samples is of considerable interest and required to respond to demands arising in different applications including point-of-care clinical testing, food analysis, process control and environmental monitoring. If biosensors or biochips are used, specific analyte detection is accomplished by biological or synthetic recognition elements, capable of identifying and binding target molecules with high specificity. These recognition elements can be employed in the form of arrays of size- and site-controlled dots in biosensors or biochips, allowing for the high-throughput detection and screening of target molecules (Lynch et al., 2004; Espina et al., 2003; Becker et al., 2007).

The recognition elements may be different biological systems including cells, organelles, enzymes, antibodies and other proteins, or deoxyribonucleic acid (DNA). Nevertheless, for some applications, these systems are inappropriate due to their instability out of their native environment. Therefore, in some cases molecularly imprinted polymers (MIPs), which are synthetic macromolecular receptors, can be used for detection (Haupt and Mosbach, 2000; Mosbach and Ramström, 1996; Wulff, 2002; Zimmerman and Lemcoff, 2004; Tokonami et al., 2009). Here, cross-linked polymers are formed around template molecules by copolymerization of functional monomers that can interact covalently or noncovalently with the template, with cross-linkers. Upon polymerization the functional groups of the monomers are frozen in their position. Following template extraction, molecular cavities are revealed, preserving a spatial arrangement complementary to the structure of the imprinted template molecule. These sites allow the polymer to rebind the template selectively from a mixture of closely related compounds, enabling MIPs to be specifically tailored for a wide range of target molecules. For their use in sensors and biochips they have to be patterned on surfaces and interfaced with optical or other transducers.

Indeed, it has been very recently shown that it is possible to fabricate a MIP microarray by mid-infrared laser pulse initiated polymerization (Henry et al., 2008). In addition, MIP droplet deposition and patterning was performed using micro-stereolithography (Conrad et al., 2003), microcantilevers (Vandevelde et al., 2007), or a nano-fountain pen (NFP) (Belmont et al., 2007), and the binding and release of target analytes was monitored by fluorescence. Although these studies demonstrated the feasibility of the approach, it is evident that fluorescence-based detection is limited to fluorescent or fluorescently labeled target molecules.

To overcome this limitation, non-labeling techniques like infrared (IR) spectroscopy (Jakusch et al., 1999; Duffy et al., 2002) or Raman spectroscopy (McStay et al., 2005; Kantarovich et al., 2009a,b; Bompart et al., 2009; Kostrewa et al., 2003), which provide vibrational spectra with high chemical and structural information content were considered. As for the latter, both spontaneous Raman scattering (Long, 1977) and surface-enhanced Raman scattering (SERS) (Fleischman et al., 1974; Jeanmaire and Vanduyne, 1977) were employed (McStay et al., 2005; Kantarovich et al., 2009a,b; Bompart et al., 2009; Kostrewa et al., 2003) for measurement of

* Corresponding author.
*E-mail address:* ibar@bgu.ac.il (I. Bar).

0956-5663/$ – see front matter © 2010 Elsevier B.V. All rights reserved.
doi:10.1016/j.bios.2010.06.018

the vibrational signatures of the adsorbed compounds in imprinted layers. These methods provide characteristic "fingerprints" allowing identification of binding or release of target molecules to and from MIPs.

Recalling that the major challenges in the field include biochip and sensor array miniaturization and their reading by non-labeling methods, we here couple the NFP method (Belmont et al., 2007; Lewis et al., 1999) for MIP droplet deposition with SERS on a nanopatterned gold surface. We show that by using this approach the binding of a template molecule, the β-blocking drug *S*-propranolol to, and its distribution in, individual droplets or in an array of droplets deposited on the SERS-active surface can be detected and imaged. The distribution of the MIP droplets was also confirmed by atomic force microscopy (AFM), showing that very low MIP volumes can be detected and identified on SERS-active substrates.

## 2. Experimental

### 2.1. Sample preparation and droplet deposition and characterization

The compounds used for MIP preparation include trimethylolpropane trimethacrylate (TRIM), methacrylic acid (MAA), diethyleneglycol dimethylether (diglyme), poly(vinyl acetate) (PVAc, MW = 140,000 g/mol), the template *S*-propranolol and 2,2-dimethoxy-2-phenyl acetophenone (DPAP). All these materials were purchased from Sigma–Aldrich, except the last one which was from Fluka. The MIPs were synthesized by UV photopolymerization from a mixture containing TRIM 0.0964 mmol, MAA 0.0964 mmol, *S*-propranolol 0.0192 mmol, DPAP 0.0195 mmol and 0.168 ml diglyme containing 2% PVAc. The NFP droplet deposition of the MIP precursors was performed under ambient conditions using a near-field scanning optical microscope/AFM (NSOM/AFM) 100 system (Nanonics) with a flat scanner and an optical microscope, enabling the examination of the sample and precise positioning of the nanopipette on the surface. NFP probes were Cr/Au covered cantilevers of 500–600 μm length and 600 nm aperture diameter (Nanonics). The nanopipette was filled from the back with the imprinting mixture, evolving to the pipette tip and flowing out only upon contact with the surface. This allowed applying minute volumes of MIP solution in selected positions on the patterned surfaces of a Klarite SERS substrate (D3 Technologies Ltd.). These SERS-active surfaces comprise gold-coated grids of pyramidal wells with 2 μm × 2 μm aperture and ~2 μm depth. Following droplet deposition in site-controlled arrays, they were polymerised in a closed compartment under argon atmosphere using a 6 W low-pressure UV lamp (254 nm, Vilber Lourmat) at a 3 cm distance from the light source, for 30 min. The polymer dots were characterized by the AFM and by SERS.

AFM characterization of the droplet morphology was performed using "Ultrasharp" gold-covered silicon contact cantilevers (Mikromasch, CSC12/CR–Au/15). AFM image analysis was done using the scanning probe image processor (SPIP™) software package from Image Metrology A/S. In some cases, the template of the imprinted polymer was eluted by incubation in ethanol/acetic acid 9:1 for 40 min, followed by a brief dipping in ethanol. The MIP samples were then re-incubated in 300 μl propranolol solution (0.03 g/l) for 40 min prior to redipping in ethanol. SERS spectra were recorded after each step.

### 2.2. Surface-enhanced Raman scattering

SERS spectra of *S*-propranolol and MIPs deposited over the Klarite substrates were collected with a micro-Raman spectrometer (LabRam UV HR, Jobin-Yvon). The 784.9 nm excitation wavelength of a diode laser was focused onto the sample with an *x*50/0.75 - numerical-aperture microscope objective, with ~10 mW intensity. The scattered light was redirected from the microscope through a sharp edge long wavepass filter, rejecting the excitation laser line and the elastically scattered light and through a 100 μm confocal pinhole for increased axial resolution. The scattered light was then focused into a 0.8 m dispersive spectrometer, equipped with a 600 groove/mm grating, and the scattered Raman light was detected with an air cooled charge-coupled device (CCD), consisting of 1024 × 256 pixels. The fingerprint region in the spectra was monitored while scanning the spectrum across the CCD and moving the grating three times. The spectral acquisition was performed following adjustment of the zero-order position of the grating and control of the Rayleigh line position of a (1 0 0) polished single-crystal silicon-wafer.

To ensure the correct position of the sample relative to the objective, an adjustment was made, based on the image observed by a TV camera monitor. Successive recordings of SERS spectra over the droplet, using a computer-controlled *x*/*y* motorized stage (Mertzhauser) with step size of 2 μm allowed measurement of the spatially dependent signatures of the MIP. The definition of the measurement parameters and measuring control was done by the LabSpec 4.04 software. All monitored spectra were smoothed.

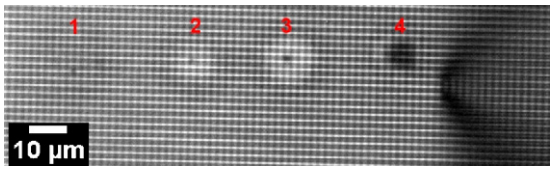


**Fig. 1.** Optical Micrograph showing the deposition of four droplets out of an array of molecularly imprinted polymer, containing the *S*-propranolol template, written with a nanopipette on a surface-enhanced Raman scattering-active surface (Klarite). The deposited droplets are marked by the numbers and in the right part the tip is observed.

## 3. Results and discussion

### 3.1. Droplets deposition

The deposition of MIP droplets on Klarite surfaces is described by the time-lapse series of images shown in Fig. 1. The droplets numbered 1–4 were deposited at ~1 s time difference, with 1 being the first and 4 being the last. It is evident that following deposition, the droplets spread over the surface, presumably due to capillary action of the patterned microwells, leaving such a thin layer that the optical contrast is lost (in droplet #1) within a few seconds. Although nanopipettes with aperture diameter of 600 nm were used for the droplet writing, the resulting droplets are of 6–12 μm in diameter. The droplets size can be controlled by modulating the contact time between the pipette and the surface, thus making it is possible to print dots.

### 3.2. Droplets characterization by surface-enhanced Raman scattering

The measured representative SERS spectrum of the free template (*S*-propranolol) includes several bands and is shown in Fig. 2(a). This spectrum differs somewhat from the regular Raman spectrum (Kantarovich et al., 2009a,b), showing broader features and higher intensity. This intensity enhancement for Klarite surfaces is a result of the localized electromagnetic field confined at the edges and in the pit, as predicted by theoretical modeling (Perney et al., 2006).

One of the structural units of propranolol is the naphthalene ring, and the most intense band in the spectrum around 1385 $cm^{-1}$

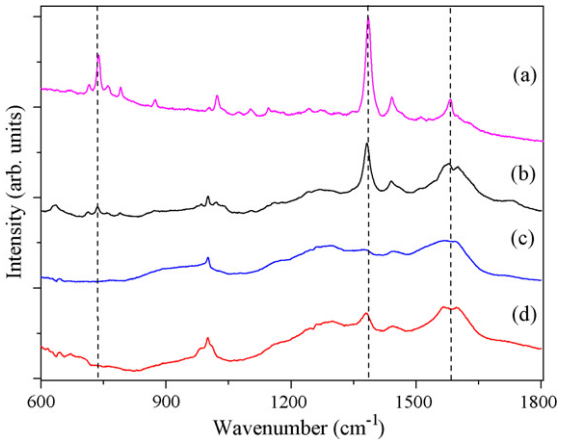


**Fig. 2.** Representative surface-enhanced Raman scattering spectra of (a) *S*-propranolol, (b) molecularly imprinted polymer (MIP), (c) extracted MIP, and (d) following rebinding of the template to the MIP. The *S*-propranolol concentration for the rebinding was 115 μM. All the spectra are of samples deposited on the Klarite surface and were measured with 40 s integration times. The spectra are plotted on the same scale and are shifted for clarity. The vertical dashed lines mark the most characteristic bands of *S*-propranolol.

(marked by the vertical dashed line) is related to it (Rupérez and Laserna, 1996). Also observed are the characteristic bands of the MIP appearing at about 736 and 1583 $cm^{-1}$ (marked by the vertical dashed lines) and several weaker bands (Kantarovich et al., 2009a,b). The SERS spectrum of *R*-propranolol was also studied, but no differences could be observed between the SERS spectra of propranolol enantiomers. This agrees with previous findings (Rupérez and Laserna, 1996) that showed that the two propranolol enantiomers give the same SERS spectra on colloidal silver.

The representative SERS spectrum of a MIP droplet like those presented in Fig. 1 is shown in Fig. 2(b). It can be clearly seen that the characteristic peak at 1385 $cm^{-1}$, reflecting the presence of the *S*-propranolol template in the imprinted polymer, is observed in the MIP as well. This band disappeared after template elution, Fig. 2(c), and reappeared following its rebinding, Fig. 2(d), although its intensity is somewhat reduced, compared to that in the MIP after synthesis [Fig. 2(b)]. As for the other characteristic bands of *S*-propranolol, it is difficult to observe the 1583 $cm^{-1}$ band in the MIP spectrum, Fig. 2(b), due to overlap with other bands, originating in other MIP constituents, but it is possible to observe the 736 $cm^{-1}$ band. This band appears in the imprinted polymer and disappears after elution, but does not reappear after rebinding, probably due to its weakness in the initially deposited MIP, Fig. 2(b). This is in line with the observation that the 1385 $cm^{-1}$ band was also reduced in intensity after rebinding, probably pointing to the fact that less *S*-propranolol was accumulated compared to the amount of template initially present in the imprinted polymer. Furthermore, this is in accordance with the widely accepted fact that the imprinting efficiency is always less than 100%, often only a few %, when noncovalent bonds are established between the imprint molecule and the monomers during imprinting. In addition, some differences are observed between the spectra of the MIP, extracted MIP and rebound MIP, implying that the SERS-active surface is somewhat affected by the chemical treatment required for the different steps. Nevertheless, the 1385 $cm^{-1}$ band is very clearly observed in the imprinted polymer as well as after rebinding and therefore, it is used for quantification of the distribution of the MIP droplet on the SERS-active surface, similarly with our previously reported approach (Kantarovich et al., 2009a,b).

However, even though we clearly see a dependence of the intensity of the SERS spectra on the concentration used during incubation, these measurements are not really quantitative since the exaltation depends on the thickness, geometry and arrangement of the MIP in the metallic nanostructures, which are inhomogeneous within one MIP dot despite the regular pattern of inverted nanopyramids in the substrate. Indeed, quantitative concentration measurements (Bell and Sirimuthu, 2008) demand high reproducibility and accurate calibration of spectral intensities, which remains a significant challenge, particularly for SERS (Sackmann and Materny, 2006). Although the reproducibility of SERS might be improved by refining the substrate fabrication procedures, it is difficult to suppress variations in intensity, spectral shape, and background. This is since the same mechanisms that are responsible for producing large local field enhancements might also lead to large variability in the Raman scattering signal. Therefore, the difference in binding that was found for the

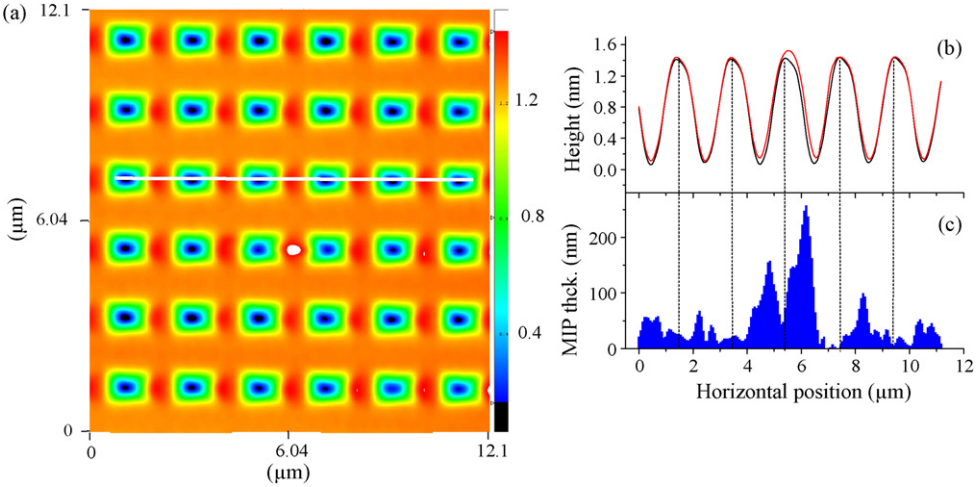


**Fig. 3.** Atomic force microscopy scan taken around the region where a droplet was deposited on the Klarite surface is shown in (a). Careful visual examination reveals that wells in the center of the image are slightly shallower than those at larger distances from the center (more molecularly imprinted polymer (MIP) is present in them). A height profile along the white line indicated in (a) is plotted in (b) (red) together with a similar profile measured in a region of the surface (black) where no deposition of MIP droplet took place. The difference between the two is plotted in (c) and represents the extent of filling of the wells by the MIP. The vertical dashed lines indicate the individual wells and help observing that the accumulation is in the well center. (For interpretation of the references to color in this figure legend, the reader is referred to the web version of the article.)

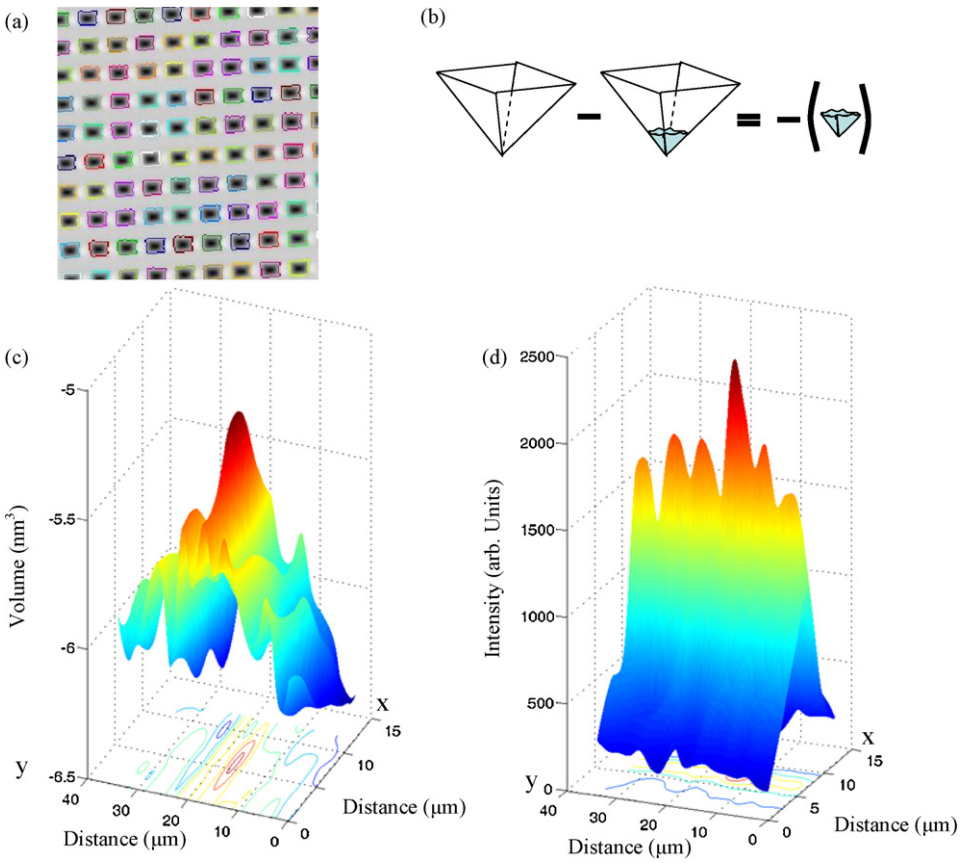


**Fig. 4.** The volumes of the molecularly imprinted polymer (MIP) in the Klarite wells as obtained by atomic force microscope (AFM) image analysis, through detection and monitoring of the individual wells (a) followed by calculation of their volumes. As presented schematically in (b), these volumes were subtracted from those of the empty wells, quantified in the same manner, to yield the volume of MIP in the particular wells. Spatial-dependent distribution of the MIP droplet on the Klarite patterned grid as obtained by AFM (c) and surface-enhanced Raman spectroscopy (d).

two enantiomers of propranolol using radioligand binding experiments (Andersson, 1996), or detection by conventional Raman spectroscopy (Kantarovich et al., 2009a,b) is likely to be masked in SERS measurements.

### 3.3. Droplet characterization by atomic force microscopy

To quantify the amount of deposited MIP, regions around the deposition positions were scanned with the AFM. A two-dimensional AFM scan across an NFP deposited MIP droplet on the SERS-active surface is shown in Fig. 3. Due to the extremely thin layer of MIP formed during the lateral spreading of drops on the rough background of Klarite microwells (~2 μm depth), it is difficult to directly observe the height profile of the deposited MIP droplet. Careful inspection of Fig. 3(a) shows that the wells in the image center are filled with MIP more than towards the image edges. An estimation of the maximal height of MIP can be obtained by taking a height profile along the deepest points of the wells, as indicated by the white line of Fig. 3(a). The profile extracted from these data is plotted in red in Fig. 3(b). A similar height profile of the Klarite surface, in a region where droplet deposition did not take place, is plotted in black in Fig. 3(b). The difference between the two patterns is plotted in Fig. 3(c) and represents the (maximum) height of MIP along this line. It can be seen that the maximum thickness of the MIP layer is ~250 nm. Also, it is clear that the MIP solution migrates to adjacent wells during and after deposition, accumulates mainly at the bottom of the wells, but obviously wets the walls as well, presumably by capillary action. This is consistent with the spreading of the droplet observed in the micrograph obtained by optical microscopy [Fig. 1]. The accumulation of the deposited MIP at the center of the well is observed by noticing the vertical dashed lines of Fig. 3 [panels (b) and (c)] which indicate the individual wells and help observing the MIP accumulation in particular wells.

### 3.4. Droplets distribution across the Klarite surface

A quantitative evaluation of the volume filled by MIP in each well was performed, using a thresholding and particle detection algorithm, available in the SPIP™ software. An area of the Klarite surface on which this approach was taken is shown in Fig. 4(a). The colored squares identify the wells, and a calculation of their volume is concomitantly performed. Subtracting these volumes from the volume of an empty well yields (minus) the volume of the MIP present in the well (see Fig. 4(b)). Based on this analysis the spatial distribution of the droplet over the wells was retrieved. This is shown in Fig. 4(c), demonstrating that the volumes of the droplet occupying each well are varying from 0.5 to 0.8 fl with a maximum in the center. Furthermore, from these results the average thickness of the MIP layer can be estimated by considering the shape of the well, which is a square-based pyramid. Therefore, extracting the cubic root of the volume and dividing it by 3, heights of ~260–300 nm were obtained, which in fact reflect the thickness of the MIP droplet. These values agree very well with the thickness obtained from the measurement of the height profile along the deepest points of the wells and with the results of Fig. 3.

The distribution of the same MIP droplet across the Klarite surface was also verified by successive monitoring of SERS spectra,

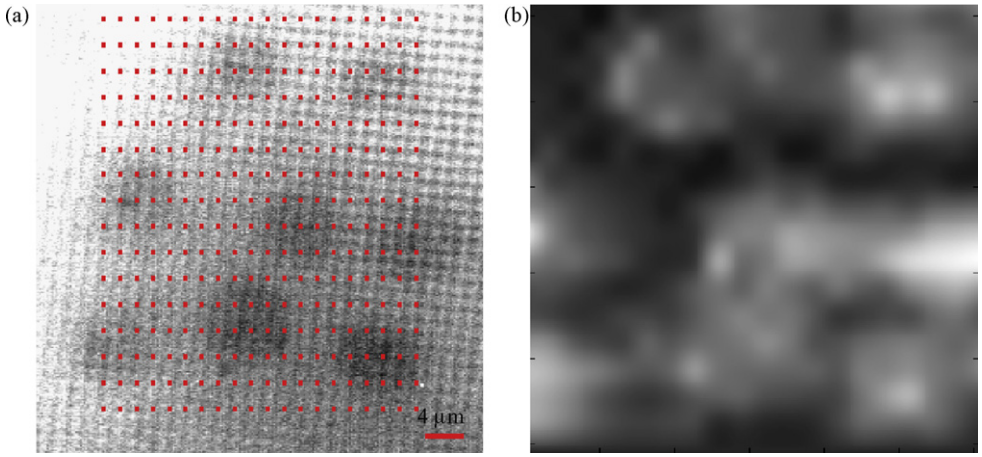


**Fig. 5.** (a) Micrograph of a MIP array on a Klarite patterned grid, where the droplets were printed by a nanopipette (~600 nm diameter). The red dots mark the measuring points of the surface-enhanced Raman scattering (SERS) spectra over the array. (b) *x*, *y* SERS map, where the white spots show the presence of MIP droplets, as obtained from the intensity distribution of the *S*-propranolol peak at 1385 $cm^{-1}$. (For interpretation of the references to color in this figure legend, the reader is referred to the web version of the article.)

while performing an *x*, *y* scan with steps of 2 μm. By calculating the 1385 $cm^{-1}$ band intensity, relative to the spectral background, the SERS intensities resulting from the MIP droplet could be obtained at each *x*, *y* position. These intensities are presented as a function of position in Fig. 4(d). Comparison of the volumes obtained by AFM [Fig. 4(c)] and the SERS intensities [Fig. 4(d)] measured for the same droplet shows a very good correspondence between them, implying that quite similar distribution of the MIP droplet is found by the two very different methods. The slight differences between the images are explained by taking into account that the SERS signal was not always measured from the pit center (since the scan step size is not commensurate with the Klarite grid spacing). It is very satisfying to find out that even very small volumes of the MIP droplet can be monitored by SERS. In addition, it should be pointed out that since the SERS excitation laser spot size on the sample is about 1 μm, it is expected that even MIP droplets of this diameter should be detectable. This could not be verified in this case due to the droplet spread and the ultimate determination of its diameter by the wetting properties of the MIP solution and the substrate.

In order to test for the applicability of the method to microbiochips, also droplets printed in an array on a Klarite surface were scanned. The optical micrograph (Fig. 5(a)) shows seven dark spots, corresponding to the deposited droplets. As can immediately be seen, each dot is around 12 μm in diameter and they are darker than the four dots of Fig. 1. The higher optical contrast of the MIP droplets in the array shows that thicker layers were deposited this time, indicating as mentioned above, that the exact characteristics of the deposited droplet are somewhat dependent on the particular nanopipette used and also on the position and contact time between the nanopipette and the surface.

By measuring SERS spectra at different measurement points over the array [small red dots in Fig. 5(a)] it was possible to obtain the spectral signatures in the particular positions. Four hundred measurements, with a distance of 2 μm between consecutive positions, were taken over the 30 μm × 38 μm pattern. The obtained spectral signatures were similar to those shown in Fig. 2(b), corresponding to the SERS spectrum of the MIP. These spectra were analyzed and the height of the *S*-propranolol peak at 1385 $cm^{-1}$, with respect to the background was measured. From these data an intensity matrix was created, leading to the *x*, *y* SERS intensity map, which was obtained by interpolation over the measured positions [see Fig. 5(b)]. Although, due to capillary action of the microwells, the MIP leaked somewhat to neighboring wells, it is clearly seen that the SERS intensities (white) of the MIP [Fig. 5(b)] correspond nicely to the droplets positions and the highest intensities match the dots in the optical image [Fig. 5(a)]. Furthermore, by integrating the intensities in each of the fully measured droplets (some are touching the edge) it was found that the variation in the SERS intensity is <10%. This implies that about the same amount of MIP appears in each spot and that the variations in the thickness of the droplets are small.

## 4. Conclusions

SERS was used to characterize an imprinted polymer, before and after extraction of the template and following template rebinding, based on bands related to the *S*-propranolol template. In addition, since NFP was used for the deposition of the droplets in arrays, miniaturization of the dots to the range of 10 μm could be obtained. SERS could be used not only for monitoring the MIP containing the *S*-propranolol template, but also to follow the distribution of the droplets printed in arrays. The distribution of the MIP droplets in the wells of the patterned surface as obtained by SERS was found to agree with the results of the AFM scan. This study shows that nanolithography techniques combined with SERS might open the possibility of miniaturized arrayed MIP sensors with label-free, specific and quantitative detection.

## Acknowledgements

K.H., L.A.G. and I.T. gratefully acknowledge financial support from the European Union (MENDOS project, Grant No. QLK4-CT2002-02323, Marie Curie Research Training Network NASCENT, Grant No. MRTN-CT-2006-33873). I.B. thanks the James Franck Binational German–Israeli Program in Laser–Matter Interaction.

## References

Andersson, L.I., 1996. Anal. Chem. 68, 111–117.
Becker, T., Hitzmann, B., Muffler, K., Pörtner, R., Reardon, K., Stahl, F., Ulber, R., 2007. Adv. Biochem. Eng./Biotechnol. 105, 249–293.
Bell, S.E.J., Sirimuthu, N.M.S., 2008. Chem. Soc. Rev. 37, 1012–1024.
Belmont, A.-S., Sokuler, M., Haupt, K., Gheber, L.A., 2007. Appl. Phys. Lett. 90, 193101-1-193101-3.
Bompart, M., Gheber, L.A., De Wilde, Y., Haupt, K., 2009. Biosens. Bioelectron. 25, 568–571.
Conrad II, P.G., Nishimura, P.T., Aherne, D., Schwartz, B.J., Wu, D., Fang, N., Zhang, X., Roberts, M.J., Shea, K.J., 2003. Adv. Mater. 15, 1541–1544.
Duffy, D.J., Das, K., Hsu, S.L., Penelle, J., Rotello, V.M., Stidham, H.D., 2002. J. Am. Chem. Soc. 124, 8290–8296.

Espina, V., Mehta, A.I., Winters, M.E., Calvert, V., Wulfkuhle, J., Petricoin III, E.F., Liotta, L.A., 2003. Proteomics 3, 2091–2100.
Fleischman, M., Hendra, P.J., McQuillan, A.J., 1974. Chem. Phys. Lett. 26, 163–166.
Haupt, K., Mosbach, K., 2000. Chem. Rev. 100, 2495–2504.
Henry, O.Y.F., Piletsky, S.A., Cullen, D.C., 2008. Biosens. Bioelectron. 23, 1769–1775.
Jakusch, M., Janotta, M., Mizaikoff, B., Mosbach, K., Haupt, K., 1999. Anal. Chem. 71, 4786–4791.
Jeanmaire, D.L., Vanduyne, R.P., 1977. J. Electroanal. Chem. 84, 1–20.
Kantarovich, K., Belmont, A.-S., Haupt, K., Bar, I., Gheber, L.A., 2009a. Appl. Phys. Lett. 94, 194103-1-194103-3.
Kantarovich, K., Tsarfati, I., Gheber, L.A., Haupt, K., Bar, I., 2009b. Anal. Chem. 81, 5686–5690.
Kostrewa, S., Emgenbroich, M., Klockow, D., Wulff, G., 2003. Macromol. Chem. Phys. 204, 481–487.
Lewis, A., Kheifetz, Y., Shambrodt, E., Radko, A., Khatchatryan, E., Sukenik, C., 1999. Appl. Phys. Lett. 75, 2689–2691.
Long, D.A., 1977. Raman Spectroscopy. McGraw-Hill, New York, USA.
Lynch, M., Mosher, C., Huff, J., Nettikadan, S., Johnson, J., Henderson, E., 2004. Proteomics 4, 1695–1702.
McStay, D., Al-Obaidi, A.H., Hoskins, R., Quinn, P.J., 2005. J. Opt. A: Pure Appl. Opt. 7, S340–S345.
Mosbach, K., Ramström, O., 1996. Biotechnology 14, 163–170.
Perney, N.M.B., Baumber, J.J., Zoorob, M.E., Charlton, M.D.B., Mahnkopf, S., Netti, C.M., 2006. Opt. Express 14, 847–857.
Rupérez, A., Laserna, J.J., 1996. Anal. Chim. Acta 335, 87–94.
Sackmann, M., Materny, A., 2006. J. Raman Spectrosc. 37, 305–310.
Tokonami, S., Shiigi, H., Nagaoka, T., 2009. Anal. Chim. Acta 641, 7–13.
Vandevelde, F., Leïchlé, T., Ayela, C., Bergaud, C., Nicu, L., Haupt, K., 2007. Langmuir 23, 6490–6493.
Wulff, G., 2002. Chem. Rev. 102, 1–27.
Zimmerman, S.C., Lemcoff, N.G., 2004. Chem. Commun., 5–14.